scientific reports

Check for updates

OPEN

Interfacial properties of SiC_f/SiC minicomposites with a scheelite coating

Na Ni[1,2]✉, Binbin Wu[2], Yinchun Shi[2], Xiaohui Fan[2] & Chuanwei Li[2]✉

Unidirectional SiC_f/SiC minicomposite with a scheelite ($CaWO_4$) interphase coating was fabricated through the precursor infiltration and pyrolysis method. Fractography of the SiC_f/SiC minicomposites indicated that weak fiber/matrix bonding can be provided by the $CaWO_4$ interphase. Furthermore, interfacial debonding stress of SiC_f/$CaWO_4$/SiC minicomposite was evaluated through the fiber push-out test, and estimated to be 80.7 ± 4.6 MPa. In-situ tensile SEM observation of SiC_f/$CaWO_4$/SiC minicomposite after oxidation at 1000–1100 °C was carried out, and thermal compatibility between $CaWO_4$ interphase coating and SiC fiber or matrix after heat treatment at 1300 °C was investigated.

Incorporation of reinforcing fibers into a brittle ceramic matrix provides a degree of pseudo-ductility to ceramic matrix composites (CMCs), typically the SiC fiber-reinforced SiC matrix composite (SiC_f/SiC), preventing catastrophic failure by several mechanisms, such as fiber debonding, fiber sliding and crack bridging. SiC_f/SiC composites are considered to be promising materials durable for severe environment applications such as super-sonic transport, space planes and fusion reactors[1–3]. The deviation of matrix cracks within the fiber-matrix interphase zone is realized and controlled by the deposition of a coating layer of a compliant material on the fibers prior to matrix fabrication[4–6]. The most effective interphase coating is considered to be PyC or BN coating[7–9]. However, the application of SiC_f/SiC composites is limited by degradation of mechanical properties in oxidizing environments, due to oxidation of the PyC or BN coating at the fiber/matrix interface, particularly at intermediate temperatures[4,10].

Alternative oxidation-resistant interphase materials such as rare-earth orthophosphate monazite ($LaPO_4$) have been considered as oxidation-resistant fiber-matrix interphases for CMCs due to the layered crystal structure and plastic deformation possibility. Studies on the $LaPO_4$ interphase showed that it could be deformed under mechanical stresses at low temperatures by twinning and dislocation[11–13]. However, it was found to be thermodynamically incompatible with SiC[14,15]. Both compatibility and oxidation resistance are important for the interphase coating to ensure the long period application of CMCs in air. Shanmugham et al. showed that a mullite interphase in SiC_f/SiC composites deflected cracks even after exposure in air at 1000 °C for 24 h[16]. Lee et al. demonstrated the use of multilayer SiO_2/ZrO_2/SiO_2 oxide coatings for SiC/SiC composites. Composite strength and crack deflection were retained after oxidation in air at 960 °C for 10 h[17]. Scheelite ($CaWO_4$) has a layered structure consisting of (WO_4) tetrahedra and eight-coordinated Ca sites and cleavage of its crystal was reported on (101) planes. The layered crystal structure and plastic deformation possibility of scheelite ($CaWO_4$) make it another potential interphase material for SiC_f/SiC composites[18–22]. So far, the fabrication of scheelite materials as the interphase coating in SiC_f/SiC composite and the investigation on its effect has not been explored.

In this work, unidirectional SiC_f/$CaWO_4$/SiC minicomposite was prepared through the precursor infiltration and pyrolysis (PIP) method. The effectiveness of the $CaWO_4$ interphase coating was investigated by comparing the fractography of SiC_f/SiC composites with and without $CaWO_4$ interphase coating. The interfacial property of the composites was quantitatively characterized by fiber push-out tests. The SiC_f/$CaWO_4$/SiC composites were oxidized at 1000–1100 °C to evaluate the oxidation resistance of the $CaWO_4$ interphase coating in oxygen-rich environments. In addition, SiC_f/$CaWO_4$/SiC composites were heat-treated at 1300 °C to investigate the compatibility between $CaWO_4$ interphase coating and SiC fiber or matrix.

[1]School of Mechanical Engineering, Shanghai Jiao Tong University, Shanghai 200240, China. [2]School of Material Science and Engineering, Shanghai Jiao Tong University, Shanghai 200240, China. ✉email: na.ni@sjtu.edu.cn; li-chuanwei@sjtu.edu.cn

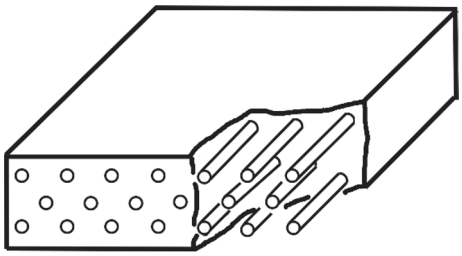

Figure 1. Schematic structure of the unidirectional SiC_f/SiC minicomposite.

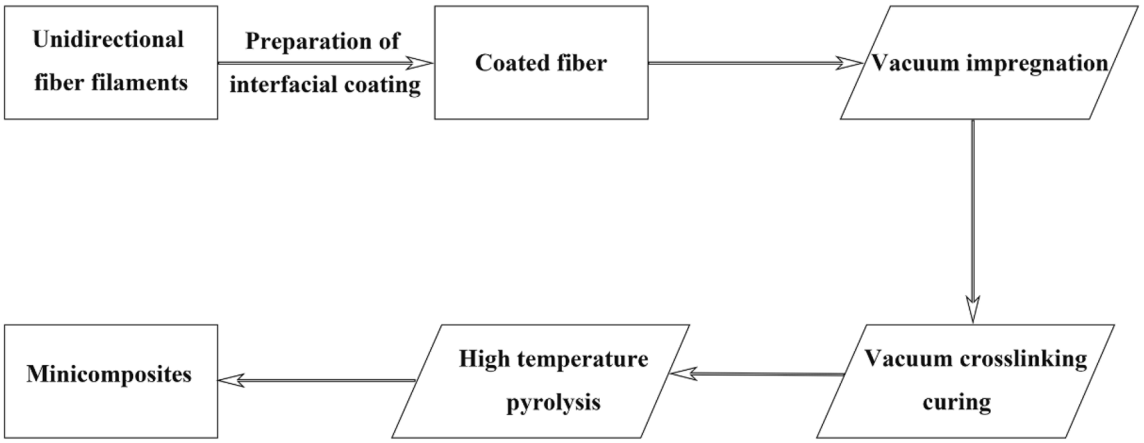

Figure 2. Preparation flow chart of SiC_f/SiC minicomposites.

Methods

Preparation of $CaWO_4$ interphase coating. Continuous $CaWO_4$ interphase coatings were prepared on KD-II SiC fiber (provided by NUDT, China) through the sol–gel method. The property of the fiber can be found in the reference[23]. The detailed coating process was described in our previous work[19,20]. The optimized firing temperature of 900℃ and atmosphere in Ar were used to avoid the fiber strength degradation during the coating process. The suitable coating thickness was obtained by repeating the coating preparation process for 6 cycles.

Preparation of SiC_f/SiC minicomposites. Unidirectional SiC_f/SiC minicomposites with and without $CaWO_4$ interphase coating were prepared through the polymer infiltration and pyrolysis (PIP) method. The schematic structure of the minicomposite is demonstrated in Fig. 1.

The flow chart for the preparation of SiC_f/SiC minicomposites is shown in Fig. 2. The PIP process utilized polycarbosilane (PCS) to form SiC matrix on pyrolysis at 1100 °C in Ar[24]. The ceramic yield of PCS is about 81–85%, and its crystallization temperature is about 1000 °C. The choice of pyrolysis temperature was based on the balance of maximum matrix densification and minimum fiber degradation. For the impregnation and crosslinking process, firstly, SiC fibers were immersed into the slender crucible which contains PCS. Then, the crucible was transferred to the vacuum drying oven to complete the vacuum impregnation process, where continuous pumping can ensure more sufficient impregnation. After pumping for 2 h, the vacuum drying oven was slowly heated up to 130 °C to complete the vacuum crosslinking curing process. Apart from that, the SiC nanoparticles (40 nm) with a volume fraction of 30–40% were filled in PCS to reduce shrinkage cracking of the matrix during pyrolysis. The infiltration and pyrolysis process was repeated 7 times to improve the density of the minicomposites.

Characterization. The composition of $CaWO_4$ coated SiC fiber tows were examined by X-ray diffractometry (XRD, Ultimo IV, Riau, Japan). Morphology of coated SiC fibers and SiC_f/SiC minicomposites was investigated by scanning electron microscopy (SEM, Inspect F50, FEI) equipped with energy dispersive spectroscopy (EDS). The porosity and density of SiC_f/SiC minicomposites were measured through Archimedes' method of drainage.

In-situ SEM observation during the tensile tests of SiCf/SiC composites was performed using an SEM (Lyra3 GMU, Tescan, Czech Republic) in combination with an in-situ tensile stage (MTEST5000W, GATAN, UK) to investigate the fracture behavior of the composites. The composite specimens used for in-situ tests were approximately $1 \times 2 \times 15$ mm in size, with their ends embedded in epoxy resin, and the area used for in-situ observation was approximately 2×4 mm. The samples were first gold sprayed (10 mA, 15 s, gold film thickness of approximately 2 nm) to increase the electrical conductivity before being placed in the SEM, and then the specimens were fixed on the tensile stage fixture (Fig. 3). In the in-situ tensile test, the stage used a displacement

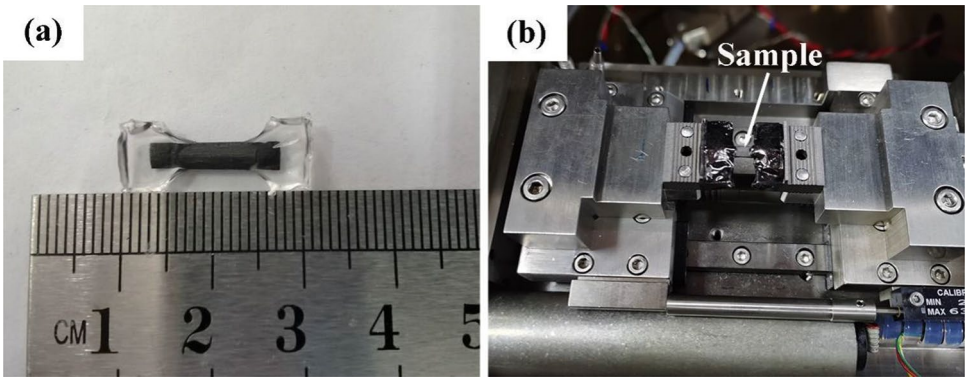

Figure 3. In-situ tensile SEM observation of SiC_f/SiC minicomposite: (**a**) sample and (**b**) tensile platform.

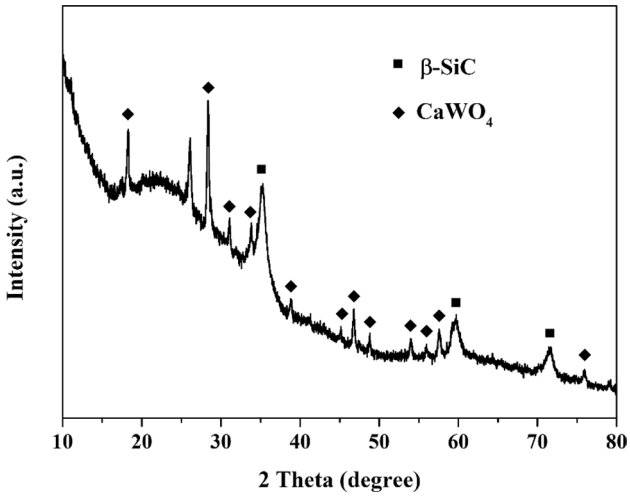

Figure 4. XRD pattern of $CaWO_4$ coated SiC fiber.

control mode, i.e., the motor loading rate was 0.1 mm/min until fracture. SEM imaging wad carried out using a backscattered electron detector with a working distance of 30 mm, a voltage of 10 kV, and beam current of 1 nA. An automatic image acquisition module with a single image acquisition time of about 3.2 s and an interval of 0 s was employed. The magnification chosen for in-situ observation was small, which can ensure that the sample was always within the field of view during the tensile process. After the sample fractured, the SEM still acquired several photographs to ensure that the whole process of stretching can be observed.

Single fiber push-out tests were carried out to quantitatively characterize the interfacial property of SiC_f/SiC minicomposites. The minicomposites were first ground and polished to 100–300 μm, and then the slice was fixed to the graphite flake with a groove. The thickness of the composite has been reported to not affect the estimation of the interfacial debonding stress[25]. Finally, Agilent Technologies G200 nano indention was utilized to push the single fiber in the composites. The maximum load is 1000 mN.

To evaluate the potential performance of the $CaWO_4$ interphase in high-temperature oxidizing environment, the SiC_f/$CaWO_4$/SiC minicomposites were oxidized at 1000–1100 °C in air for 10 h and 50 h in the muffle furnace (SXL-1400). Furthermore, the composites were heat-treated at higher temperatures of 1200–1300 °C for 10 h and 50 h in air to investigate the compatibility between the $CaWO_4$ coating and SiC.

Results and discussion

Characterization of $CaWO_4$ coated fibers and minicomposites. According to the XRD analysis of $CaWO_4$ coated SiC fiber shown in Fig. 4, only $CaWO_4$ was identified besides the β-SiC phase originating from the underlying SiC fiber, suggesting that the prepared interphase coating is pure $CaWO_4$.

Figure 5 shows the surface morphology of the coated SiC fiber. Together with XRD, it can be confirmed that $CaWO_4$ interphase coating was successfully prepared on SiC fibers. If compared to interphase coating fabricated by CVD methods, e.g. BN coating in[7], the $CaWO_4$ interphase coating prepared by the so-gel method is relatively rougher.

The size of the unidirectional SiC_f/SiC minicomposite prepared by the PIP method is about $2 \times 3 \times 20$ mm. The cross-section view of SiC_f/SiC minicomposites (SEM backscattered electron images) with and without the

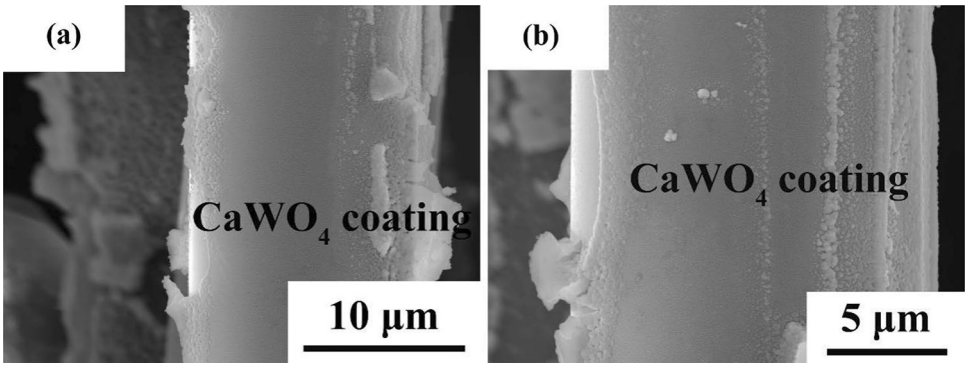

Figure 5. Surface morphology of $CaWO_4$ coated SiC fiber.

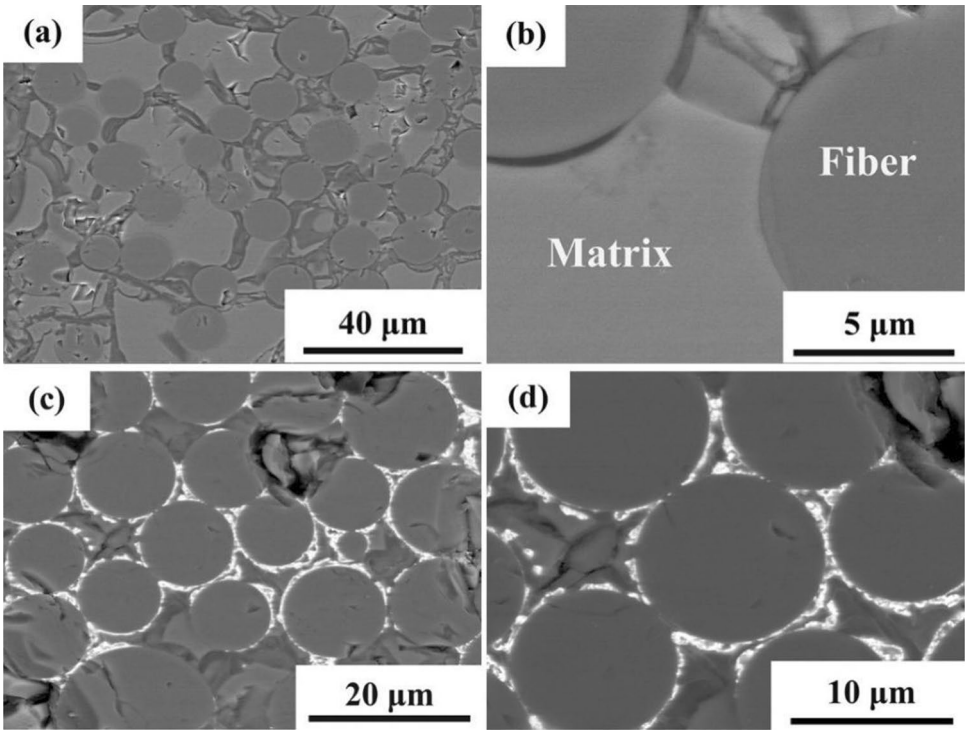

Figure 6. Cross-section view of SiC_f/SiC minicomposites: (**a**,**b**) without interphase coating and (**c**,**d**) with $CaWO_4$ interphase coating.

$CaWO_4$ interphase coating is demonstrated in Fig. 6. As shown in Figs. 5, 6, there exist regions around the fiber with no interphase coating. Mud cracks often observed in composites prepared by the PIP method[26] were also found in the current SiC_f/SiC minicomposites as shown in Fig. 6. According to Fig. 6c,d, in the coated area the $CaWO_4$ interphase coatings have a thickness in the range of 200–600 nm.

The density of SiC_f/SiC minicomposites with and without the $CaWO_4$ interphase coating is about 2.16 g/cm^3 and 2.29 g/cm^3, respectively, and their porosity is about 14.4% and 10% respectively. The higher porosity of SiC_f/SiC composites with the $CaWO_4$ interfacial coating is probably due to its influence on the impregnation efficiency of PCS. The distribution of $CaWO_4$ interphase coating prepared through sol–gel method is relatively random and liable to aggregate on the fiber surface, which may obstruct the impregnation of PCS. The lower impregnation efficiency of PCS can cause less SiC matrix filled inside the fiber tow, which leads to the higher porosity of the SiC_f/SiC minicomposite.

Interfacial property of minicomposites. As one of the main functions of the interphase coating is to render pseudoplasticity to the composites, it is necessary to study the fracture behavior of the interphase-modified composite. As the prepared minicomposite samples were too small for carrying out reliable macroscopic tensile tests, the effect of the $CaWO_4$ interphase coating on fracture behavior of SiC_f/SiC minicomposites was

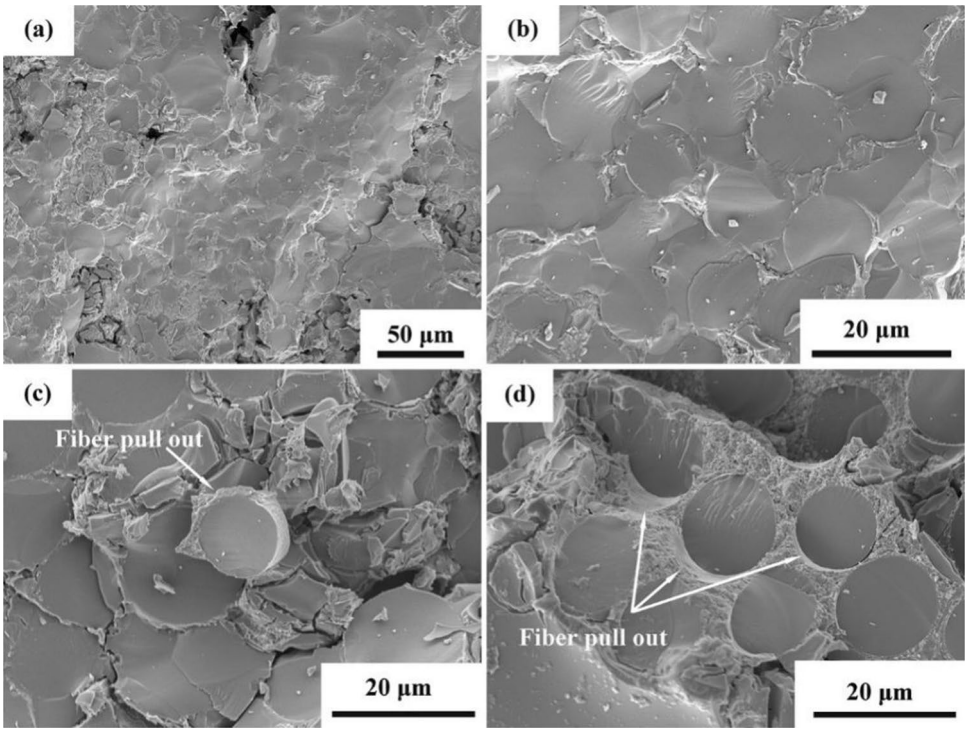

Figure 7. High-magnification fracture surface of SiC_f/SiC minicomposites: (**a**,**b**) without interphase coating and (**c**,**d**) with $CaWO_4$ interphase coating.

mainly investigated by comparing the SEM fractography of the composite with and without the interphase. Fracture surfaces of the minicomposites are demonstrated in Fig. 7. The fracture surfaces of the minicomposite were generated through the in-situ tensile test as described in the experimental section. Flat fracture surfaces were obtained for the minicomposite without interphase coatings, and indications of crack deflection at the fiber/matrix interface or fiber pullout were not found (Fig. 7a,b). The SEM examination of the minicomposite without the interphase coating suggests clearly a brittle failure.

In the case of minicomposites reinforced with $CaWO_4$ coated fibers, a rugged fracture surface was found. Debonding was observed to occur at the fiber/matrix interface, and distinct fiber pullouts were found on the fracture surface (Fig. 7c). In addition, SEM observation showed trough formation in the matrix after fiber pullout (Fig. 7d).

By comparing the fracture surface of SiC_f/SiC minicomposites with and without $CaWO_4$ interphase coating, it is indicated that $CaWO_4$ interphase coating has a positive effect in changing the fracture behavior from a brittle manner to a more ductile one. When no interphase coating is present at the fiber/matrix interface, a strong bonding is formed, and as a result, cracks penetrate the fibers without any deflection during the failure of composites[27–29]. Hence, a flat fracture surface was obtained suggesting minimal fracture energy. In the SiC_f/$CaWO_4$/SiC minicomposite, the existence of $CaWO_4$ interphase coating can provide a weaker interface bonding promoting the fiber/matrix interface debonding and fiber pullout during failure. Consequently, a rugged fracture surface was formed associated with the consumption of higher fracture energies.

The effect of the $CaWO_4$ coating on the interfacial property of the minicomposites is further evaluated quantitatively through the fiber push-out test. Fibers located above the groove and surrounded by the matrix were chosen randomly for push-out tests. To facilitate the push-out experiment accounting for the potentially stronger fiber/matrix bonding, the SiC_f/SiC minicomposites without interphase coating were ground and polished to a thinner slice allowing the use of lower push-out loads. Figure 8 shows the typical indentation curve of SiC_f/SiC minicomposites with (Fig. 8a) and without interphase coating (Fig. 8b) obtained from the single fiber push-out test. A similar single fiber push-out curve was reported by Zhang et al. [25]. According to the load–displacement curve, the push-out process of a single fiber in the SiC_f/$CaWO_4$/SiC minicomposite can be divided into four periods (A, B, C, and D) which were marked in the indentation curve (Fig. 8). Figure 9 indicates a schematic diagram of these four periods in the fiber push-out process[25].

In period A, the indenter presses into the SiC fiber, and the elastic deformation of SiC fiber occurs. The fiber/matrix interface is still in good condition with no cracks formed at the interface. During this period, the impact energy of the indenter is entirely assimilated by the elastic deformation of the SiC fiber[25]. In period B, partial debonding occurs at the fiber/matrix interface, and small cracks are formed at the interface caused by the decoupling of fiber and matrix. As a result, Young's modulus of the fiber/matrix system decreases as shown in Fig. 8. In period C, the fiber/matrix interface is entirely debonded. The fiber push-out is initiated and then SiC fiber is pushed below the surface of the slice. The critical load when SiC fiber is pushed out is denoted as, P_{max}

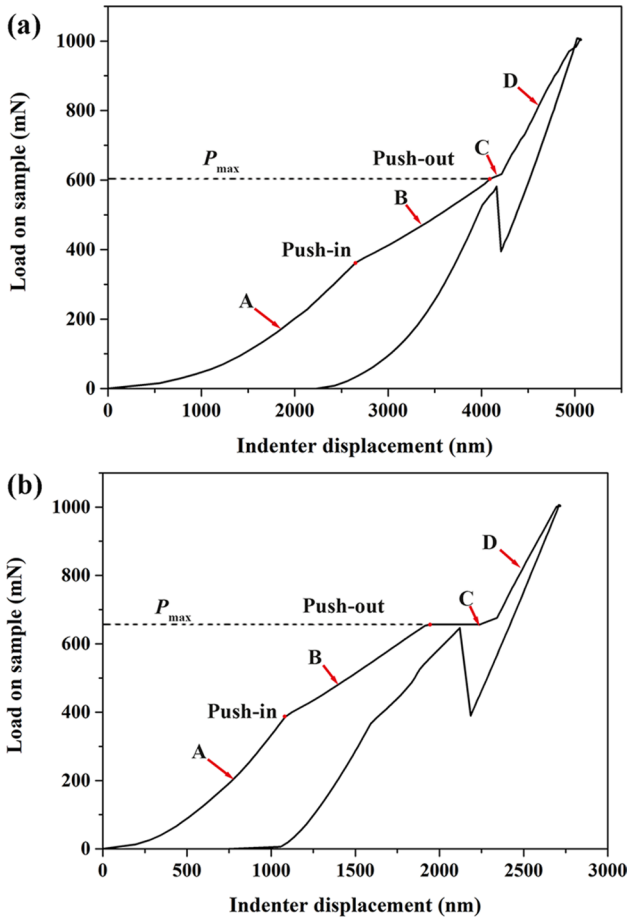

Figure 8. Representative indentation curve of single-fiber push-out tests on the SiC_f/SiC minicomposite: (**a**) with $CaWO_4$ interphase coating and (**b**) without interphase coating.

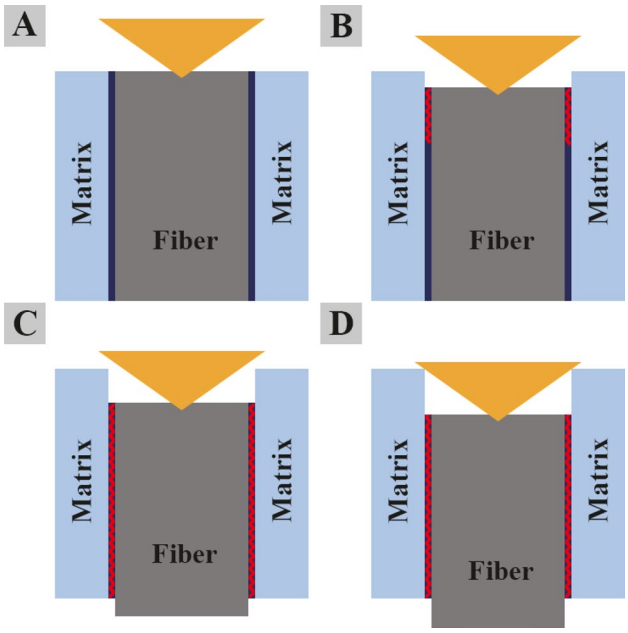

Figure 9. Schematic diagram of the fiber push-out process loaded by nanoindentation performed on the SiC_f/$CaWO_4$/SiC minicomposite. Adapted from reference[25].

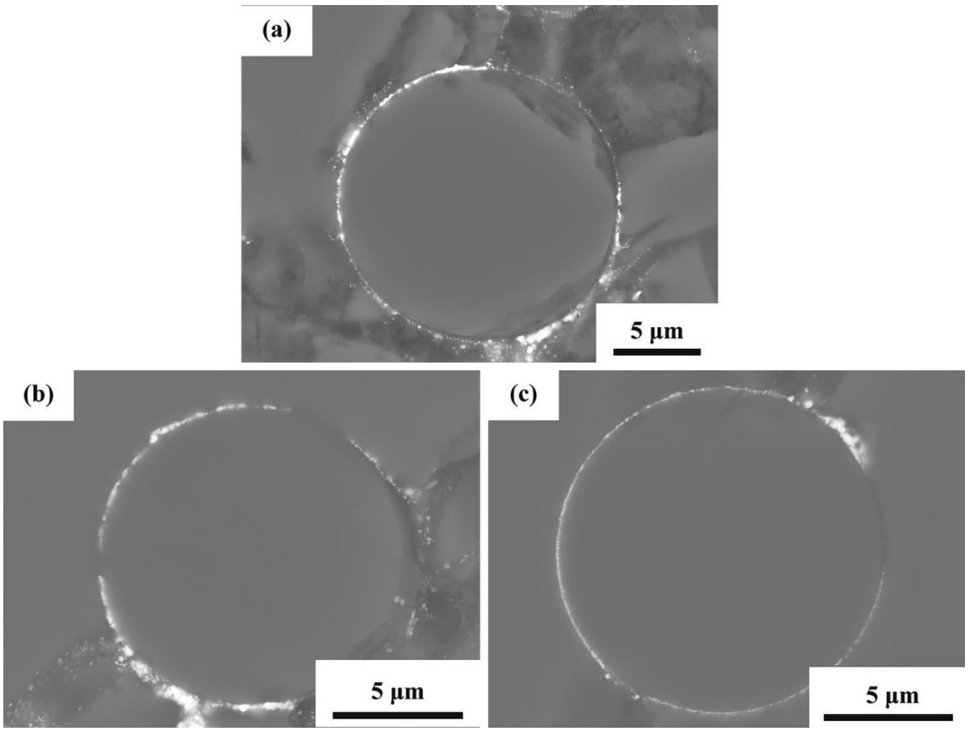

Figure 10. Cross-section view of $SiC_f/CaWO_4/SiC$ minicomposites oxidized at (**a**) 1000 °C for 50 h, (**b**) 1100 °C for 10 h, and (**c**) 1100 °C for 50 h.

(Fig. 8). Finally, in period D, the indenter touches the surrounding SiC matrix causing the increase of Young's modulus of the system.

The interfacial debonding stress of $SiC_f/CaWO_4/SiC$ minicomposite can be calculated as follows[30,31]

$$\tau = \frac{P_{max}}{\pi DL} \tag{1}$$

where τ is the interfacial debonding stress, P_{max} the push-out load, D the diameter of SiC fiber, and L the thickness of the slice.

About 15 push-out tests were carried out for the minicomposite. The average interfacial debonding stress of SiC_f/SiC minicomposite with $CaWO_4$ interphase coating and without interphase coating is calculated to be 80.7 ± 4.6 and 130.7 ± 0.1 MPa respectively, using Eq. (1). The interfacial debonding stress of composites with BN and PyC coating is about 5–20 MPa[32,33], and the debonding stress of composites with $LaPO_4$ interphase is about 100–200 MPa[34,35]. Lower interfacial debonding stress represents a weaker interface bonding and facilitates the toughening of the composites. Hence, the effectiveness of $CaWO_4$ interphase for toughening is likely to be worse than BN or PyC coating but slightly better or close to the $LaPO_4$ coating.

Based on the fracture surface investigation and interfacial debonding stress measurements, it is evident that the $CaWO_4$ interphase indeed improved the interfacial property by providing a weaker bonding at the orginal fiber/matrix interface. It is noted, however, that the toughnening effect is not dramastic in the current work as indicated by the limited debonding length and matrix cracking observed from the fracture surface. This should be at least partly due to the localized incompleteness of the coating as seen in Fig. 6. It is believed that future optimization of the coating process would enable a complete utilization of the toughening effect provided by the $CaWO_4$ interphase.

Effect of oxidation on the interphase and composite. The $SiC_f/CaWO_4/SiC$ minicomposite was oxidized at 1000 °C for 50 h and 1100 °C for 10 h and 50 h, and the cross-section view of the oxidized minicomposites is demonstrated in Fig. 10. According to the SEM observation, the $CaWO_4$ interphase coating was still visible in the composite after the oxidation process, confirming that the $CaWO_4$ interphase coating has a good oxidation resistance as expected. Hence, it can be speculated that $CaWO_4$ interphase coating would be able to promote crack deflection and fiber pullout in the oxygen-rich environment for a long time.

In-situ tensile SEM observation of the $SiC_f/CaWO_4/SiC$ minicomposite after being oxidized at 1100 °C for 50 h was carried out to evaluate the effectiveness of $CaWO_4$ interphase coating after oxidation. Unoxidized SiC_f/SiC minicomposite without the interphase coating was also investigated for comparison. SEM micrographs obtained in-situ during the tensile testing of the SiC_f/SiC and oxidized $SiC_f/CaWO_4/SiC$ minicomposite are shown in Figs. 11, 12, respectively. The entire failure process of SiC_f/SiC minicomposite was completed within less than 2 s. It is obvious that the crack propagation path of SiC_f/SiC minicomposite is almost perpendicular to the upper

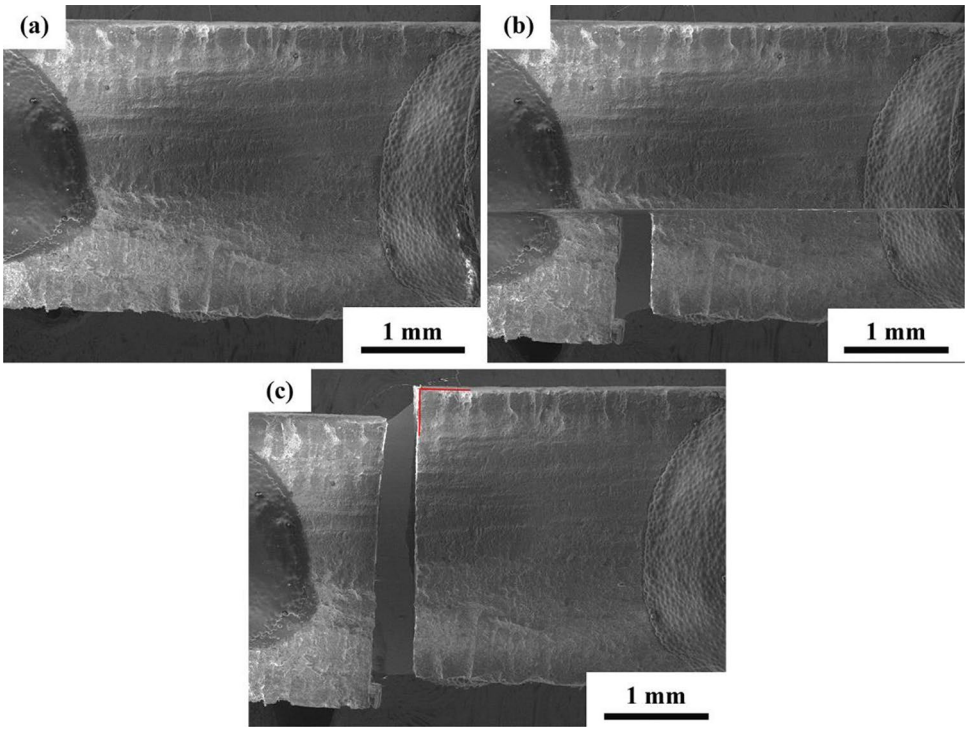

Figure 11. In-situ tensile SEM observation of SiC_f/SiC minicomposite without interphase coatings.

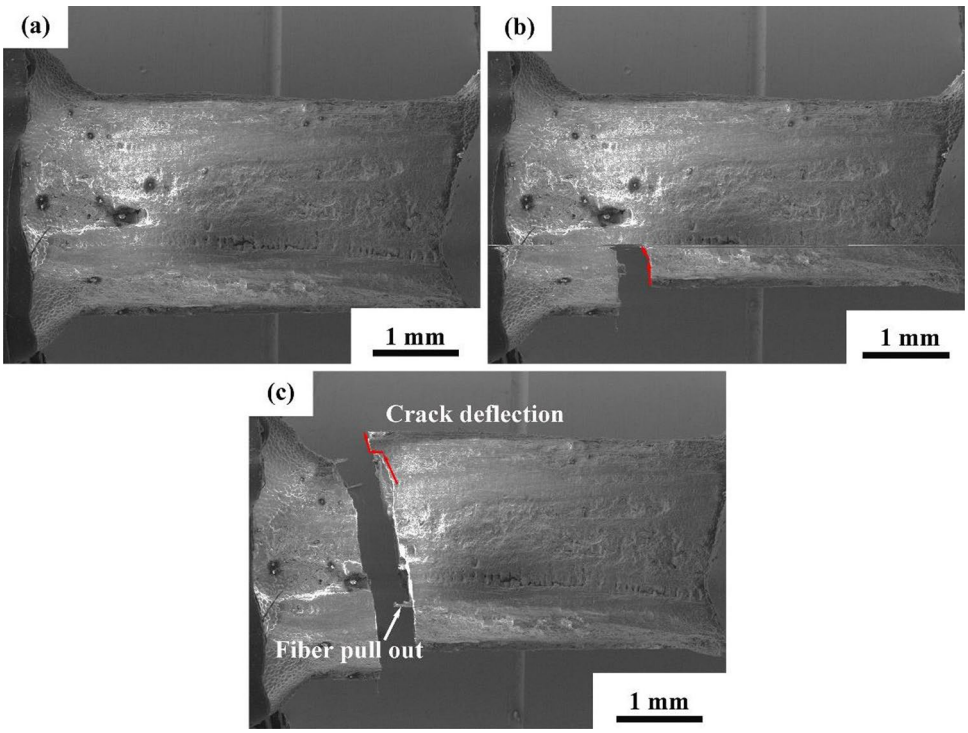

Figure 12. In-situ tensile SEM observation of $SiC_f/CaWO_4$/SiC minicomposite oxidized at 1100℃ for 50 h.

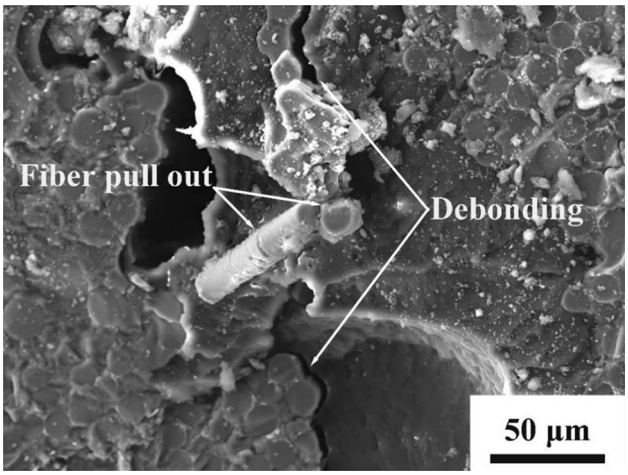

Figure 13. Fractography of $SiC_f/CaWO_4/SiC$ minicomposite oxidized at 1100 °C for 50 h.

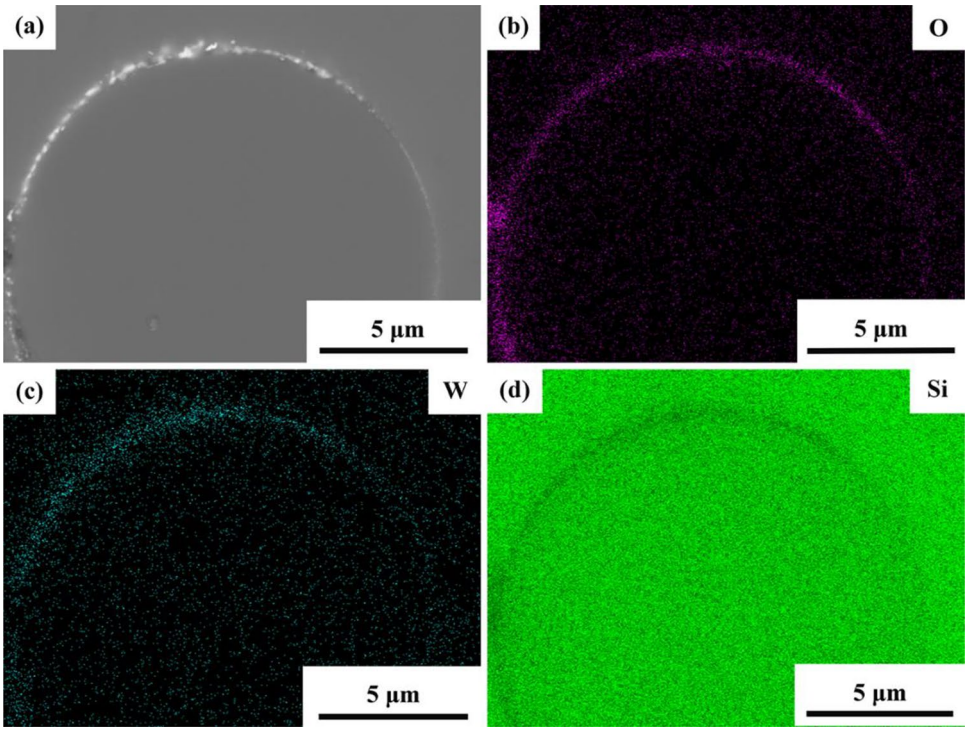

Figure 14. (**a**) Cross-section view of $SiC_f/CaWO_4/SiC$ minicomposite heat-treated at 1300 °C for 50 h. (**b**–**d**) Corresponding EDS map scanning results.

and lower surfaces of the composite, and the crack penetrates the fibers without any deflection (Fig. 11). The flat fracture surface of SiC_f/SiC minicomposite is in accordance with the fracture surface morphology shown in Fig. 6.

In comparison, crack deflection and apparent fiber pullout were indicated during the failure of $SiC_f/CaWO_4/SiC$ minicomposite that has been oxidized at 1100 °C for 50 h (Fig. 12). Figure 13 further shows the fractography of $SiC_f/CaWO_4/SiC$ minicomposite oxidized at 1100 °C for 50 h. Fiber pullout and fiber/matrix interface debonding were observed on the fracture surface which confirms that the $CaWO_4$ interphase coating remains effective in toughening the minicomposite after oxidation. This is in high contrast to the PyC and BN coating, which are prone to be consumed by oxidation at intermediate temperatures leading to strong bonding at the fiber/matrix interface and the loss of crack deflection functionality[36,37].

Thermal compatibility between $CaWO_4$ and SiC. The $SiC_f/CaWO_4/SiC$ minicomposite was heat-treated at a higher temperature of 1300 °C for 50 h to evaluate the thermal compatibility between $CaWO_4$ and SiC. The cross-section image and corresponding EDS map from the interface area are shown in Fig. 14. The

$CaWO_4$ interphase coating remains visible at the fiber/matrix interface and no obvious reaction zone is found between interphase and fiber or matrix. Meanwhile, the EDS mapping indicates the absence of Si in the interphase and W or O in the SiC matrix or fiber, which further confirms that no interfacial reaction happens after the heat treatment at 1300 °C for 50 h. Compared with the $LaPO_4$ coating that has been shown reacting with SiC at 1200 °C[15], the good thermal compatibility between $CaWO_4$ interphase and SiC at 1300 °C suggests that $CaWO_4$ interphase is more suitable for SiC_f/SiC composites.

Conclusions

Relatively uniform $CaWO_4$ interphase coatings were prepared on the SiC fiber using the sol–gel dip-coating method and unidirectional $SiC_f/CaWO_4$/SiC minicomposites were then fabricated through the PIP method. The thickness of the interphase coating was in the range of 200–600 nm. The interfacial property of $SiC_f/CaWO_4$/SiC minicomposite was quantitatively evaluated and the thermal stability of $CaWO_4$ interphase coating at 1000–1300 °C in air was investigated. The results are summarized as:

(1) Crack deflection and fiber pullout are observed during the failure of the $SiC_f/CaWO_4$/SiC minicomposite, indicating that a weak fiber/matrix interface is provided by $CaWO_4$ interphase coating. The interfacial debonding stress of SiC_f/SiC minicomposite with the $CaWO_4$ interphase coating is about 80.7 ± 4.6 MPa which is between that of PyC and $LaPO_4$ coating.
(2) Different from PyC and BN coating, the CaWO4 interphase coating is confirmed to have a good oxidation resistance. The $CaWO_4$ interphase coating is preserved at the interface and can promote crack deflection and fiber pullout after the composite is oxidation at 1000–1100 °C for 10–50 h.
(3) The $CaWO_4$ interphase coating has no obvious interfacial reaction and diffusion with SiC fiber or matrix after heat treatment at 1300 °C for 50 h, suggesting its better thermal compatibility with SiC than the $LaPO_4$ coating. Combined with the suitable interphase bonding stress, the $CaWO_4$ interphase coating has a good potential to be used in SiC_f/SiC composites.

Data availability

Datasets used or analyzed during the current study are available from the corresponding author on a reasonable request.

Received: 13 August 2022; Accepted: 16 December 2022
Published online: 19 December 2022

References

1. Snead, L. L., Jones, R. H., Kohyama, A. & Fenici, P. Status of silicon carbide composites for fusion. *J. Nucl. Mater.* **233–237**(part-P1), 26–36 (1996).
2. Hinoki, T., Zhang, W., Kohyama, A., Sato, S. & Noda, T. Effect of fiber coating on interfacial shear strength of SiC/SiC by nano-indentation technique. *J. Nucl. Mater.* **258**, 1567–1571 (1998).
3. Yoshida, K., Matsukawa, K., Imai, M. & Yano, T. Formation of carbon coating on SiC fiber for two-dimensional SiC f/SiC composites by electrophoretic deposition. *Mater. Sci. Eng. B* **161**(1), 188–192 (2009).
4. Kerans, R. J., Hay, R. S., Parthasarathy, T. A. & Cinibulk, M. K. Interface design for oxidation-resistant ceramic composites. *J. Am. Ceram. Soc.* **85**(11), 2599–2632 (2002).
5. Chen, S. A., Zhang, Y., Zhang, C., Dan, Z. & Zhang, Z. Effects of SiC interphase by chemical vapor deposition on the properties of C/ZrC composite prepared via precursor infiltration and pyrolysis route. *Mater. Des.* **46**(4), 497–502 (2013).
6. Chen, S. *et al.* Effects of polymer derived SiC interphase on the properties of C/ZrC composites. *Mater. Des.* **58**, 102–107 (2014).
7. Sun, E. Y., Lin, H. T. & Brennan, J. J. Intermediate-temperature effects on boron nitride-coated silicon carbide-fiber-reinforced glass-ceramic composites. *J. Am. Ceram. Soc.* **80**(3), 609–614 (2010).
8. Naslain, R. *et al.* Boron nitride interphase in ceramic-matrix composites. *J. Am. Ceram. Soc.* **74**(10), 2482–2488 (1991).
9. Tressler, R. E., Messing, G. L., Pantano, C. G. & Newnham, R. E. *Tailoring Multiphase and Composite Ceramics* (Springer, 2012).
10. Cofer, C. G. & Economy, J. Oxidative and hydrolytic stability of boron nitride — A new approach to improving the oxidation resistance of carbonaceous structures. *Carbon* **33**(94), 389–395 (1995).
11. Davis, J. B., Hay, R. S., Marshall, D. B., Morgan, P. & Sayir, A. Influence of interfacial roughness on fiber sliding in oxide composites with la-monazite interphases. *J. Am. Ceram. Soc.* **86**, 305–316 (2003).
12. Fair, G. E., Hay, R. S. & Boakye, E. E. Precipitation coating of monazite on woven ceramic fibers: I. Feasibility. *J. Am. Ceram. Soc.* **90**(2), 448–455 (2007).
13. Fair, G. E. *et al.* Precipitation coating of monazite on woven ceramic fibers: III—Coating without strength degradation using a phytic acid precursor. *J. Am. Ceram. Soc.* **93**(2), 420–428 (2010).
14. Boakye, E. E. *et al.* Monazite coatings on SiC fibers I: Fiber strength and thermal stability. *J. Am. Ceram. Soc.* **89**(11), 3475–3480 (2006).
15. Cinibulk, M. K., Fair, G. E. & Kerans, R. J. High-temperature stability of lanthanum orthophosphate (Monazite) on silicon carbide at low oxygen partial pressures. *J. Am. Ceram. Soc.* **91**, 2290–2297 (2010).
16. Shanmugham, S., Stinton, D. P., Rebillat, F., Bleier, A., Besmann, T. M., Lara-Curzio, E., Liaw, P. K. Oxidation-resistant interfacial coatings for continuous fiber ceramic composites. In *Proceedings of the 19th Annual Conference on Composites, Advanced Ceramics, Materials, and Structures-A: Ceramic Engineering and Science Proceedings*, Vol. 16.
17. Lee, W. Y., Lara-Curzio, E. & More, K. L. Multilayered oxide interphase concept for ceramic-matrix composites. *J. Am. Ceram. Soc.* **81**(3), 717–720 (1998).
18. Mogilevsky, P., Parthasarathy, T. A. & Petry, M. D. Anisotropy in room temperature microhardness and fracture of CaWo4 scheelite. *Acta Mater.* **52**(19), 5529–5537 (2004).
19. Wu, B., Ni, N., Fan, X., Zhao, X. & Xiao, P. Scheelite coatings on SiC fiber: Effect of coating temperature and atmosphere. *Ceram. Int.* **47**(2), 1693–1703 (2021).
20. Wu, B. *et al.* Strength retention in scheelite coated SiC fibers: Effect of the gas composition and pre-heat treatment. *J. Eur. Ceram. Soc.* **40**(8), 2801–2810 (2020).

21. Hay, R. S. Monazite and scheelite deformation mechanisms. In *24th Annual Conference on Composites, Advanced Ceramics, Materials, and Structures: B: Ceramic Engineering and Science Proceedings*, 203–217 (2000).
22. Goettler, R. W., Sambasivan, S., Dravid, V. P. Isotropic complex oxides as fiber coatings for oxide-oxide CFCC. In *Proceedings of the 21st Annual Conference on Composites, Advanced Ceramics, Materials, and Structures—A: Ceramic Engineering and Science Proceedings*, 279–284 (1997).
23. Chai, Y., Zhou, X. & Zhang, H. Effect of oxidation treatment on KD–II SiC fiber–reinforced SiC composites. *Ceram. Int.* **43**(13), 9934–9940 (2017).
24. Huang, Z., Dong, S., Yuan, M. & Jiang, D. Manufacturing 2D carbon-fiber-reinforced SiC matrix composites by slurry infiltration and PIP process. *Ceram. Int.* **34**, 1201–1205 (2008).
25. Zhang, L., Ren, C., Zhou, C., Xu, H. & Jin, X. Single fiber push-out characterization of interfacial mechanical properties in unidirectional CVI-C/SiC composites by the nano-indentation technique. *Appl. Surf. Sci.* **357**(DEC.1PT.B), 1427–1433 (2015).
26. Zok, F. W. Ceramic-matrix composites enable revolutionary gains in turbine engine efficiency. *Am. Ceram. Soc. Bull.* **95**(5), 22–28 (2016).
27. Boakye, E. E. *et al.* Evaluation of SiC/SiC minicomposites with yttrium disilicate fiber coating. *J. Am. Ceram. Soc.* **101**(1), 91–102 (2018).
28. Chawla, K. K. *Ceramic Matrix Composites* 212–251 (Springer, 1998).
29. Krenkel, W. *Ceramic Matrix Composites: Fiber Reinforced Ceramics and Their Applications* (Wiley, 2008).
30. Yang, W., Kohyama, A., Noda, T., Katoh, Y. & Yu, J. Interfacial characterization of CVI-SiC/SiC composites. *J. Nucl. Mater.* **307**(2), 1088–1092 (2002).
31. Tandon, G. P. & Pagano, N. J. Micromechanical analysis of the fiber push-out and re-push test. *Compos. Sci. Technol.* **58**(11), 1709–1725 (1998).
32. Cao, H. *et al.* Effect of interfaces on the properties of fiber-reinforced ceramics. *J. Am. Ceram. Soc.* **73**(6), 1691–1699 (1990).
33. Curtin, W. A., Eldridge, J. I. & Srinivasan, G. V. Push-out tests on a new silicon carbide/reaction-bonded silicon carbide ceramic matrix composite. *J. Am. Ceram. Soc.* **76**(9), 2300–2304 (1993).
34. Morgan, P. E. & Marshall, D. B. Ceramic composites of monazite and alumina. *J. Am. Ceram. Soc.* **78**(6), 1553–1563 (1995).
35. Kuo, D.-H., Kriven, W. M. & Mackin, T. J. Control of interfacial properties through fiber coatings: Monazite coatings in oxide-oxide composites. *J. Am. Ceram. Soc.* **80**(12), 2987–2996 (1997).
36. Wang, L. Y., Luo, R. Y., Cui, G. Y. & Chen, Z. F. Oxidation resistance of SiCf/SiC composites with a PyC/SiC multilayer interface at 500 °C to 1100 °C. *Corros. Sci.* **167**, 108522 (2020).
37. Bertrand, S., Pailler, R. & Lamon, J. Influence of strong fiber/coating interfaces on the mechanical behavior and lifetime of Hi-Nicalon/(PyC/SiC)n/SiC minicomposites. *J. Am. Ceram. Soc.* **84**, 787–794 (2001).

Acknowledgements

This work was supported by the National Natural Science Foundation of China (No. 52072238).

Author contributions

N.N and B.B.W designed and performed the experiments, and analyzed the data. N.N and C.W.L supervised this study. All the authors discussed the results., and wrote and reviewed the manuscript text.

Competing interests

The authors declare no competing interests.

Additional information

Correspondence and requests for materials should be addressed to N.N. or C.L.

Reprints and permissions information is available at www.nature.com/reprints.

Publisher's note Springer Nature remains neutral with regard to jurisdictional claims in published maps and institutional affiliations.

Open Access This article is licensed under a Creative Commons Attribution 4.0 International License, which permits use, sharing, adaptation, distribution and reproduction in any medium or format, as long as you give appropriate credit to the original author(s) and the source, provide a link to the Creative Commons licence, and indicate if changes were made. The images or other third party material in this article are included in the article's Creative Commons licence, unless indicated otherwise in a credit line to the material. If material is not included in the article's Creative Commons licence and your intended use is not permitted by statutory regulation or exceeds the permitted use, you will need to obtain permission directly from the copyright holder. To view a copy of this licence, visit http://creativecommons.org/licenses/by/4.0/.

© The Author(s) 2022